Frontiers of Information Technology & Electronic Engineering
www.jzus.zju.edu.cn; engineering.cae.cn; www.springerlink.com
ISSN 2095-9184 (print); ISSN 2095-9230 (online)
E-mail: jzus@zju.edu.cn

Correspondence:

An orbital angular momentum multiplexing communication system at 28 GHz with an active uniform circular array*#

Yu GAN[1], Lin LIU[2], Jian BAI[2], Hongfu MENG†‡[1]

[1]*State Key Laboratory of Millimeter Waves, School of Information Science and Engineering, Southeast University, Nanjing 210096, China*

[2]*Beijing Remote Sensing Equipment Research Institute, Beijing 100071, China*

†E-mail: menghongfu@163.com

Received May 10, 2024; Revision accepted Nov. 7, 2024; Crosschecked Dec. 30, 2024

https://doi.org/10.1631/FITEE.2400376

This paper presents an orbital angular momentum (OAM) multiplexing communication system employing active uniform circular arrays (UCAs) to achieve simultaneous five-mode transmission. At 28 GHz, dual-loop UCAs are implemented in the transceiver, in which four UCAs comprising multiple 4×4 microstrip subarrays are placed concentrically. The next stage of each channel is an active transmitter and receiver (T/R) module, which is composed of a beamformer integrated circuit (IC) and a feed network. Additionally, a central antenna with the ability to transmit mode 0 is integrated. Similar to the active phased array system, both the receiving and transmitting modes are reconfigurable by adjusting the phase shifter. According to specific requirements, the modes of different UCAs can be assigned arbitrarily, and the receiving and transmitting states of each UCA can be configured independently. In this study, a 6-m OAM link with data transmission rate of 3 Gbit/s has been successfully implemented.

1 Introduction

The surge in data traffic and the relentless demand for high-capacity wireless transmission have driven researchers to explore innovative techniques to enhance spectral efficiency and transmission capacity. Point-to-point free-space communication links, particularly for indoor, data center, and front-haul and back-haul systems, offer a promising solution. Among these techniques, spatial multiplexing stands out as an efficient approach to boosting the capacity of wireless systems. Multi-input multi-output (MIMO) systems (Gesbert et al., 2003) and OAM multiplexing (Gibson et al., 2004; Yousif et al., 2019; Zhang et al., 2021) are two notable examples that have garnered significant attention in recent years.

The fundamental antennas used for generating OAM waves include helicoidal parabolic antennas and spiral phase plates (SPPs) (Yan et al., 2014). SPPs have demonstrated effective wireless transmission at 60 GHz, achieving a data rate of 32 Gbit/s. Polarization-division multiplexing (Qiu et al., 2023) and intelligent surfaces (Cheng et al., 2023; Yang et al., 2023) can also be used for OAM multiplexing communication. However, their capacity is limited to the generation of a singular OAM mode. Planar reflectarrays present an innovative alternative to replace the large helicoidal parabolic reflector (Tamburini et al., 2015). Meanwhile, the UCA is a widely adopted technique for generating

‡ Corresponding author

* Project supported by the National Natural Science Foundation of China (No. 61101020)

Electronic supplementary materials: The online version of this article (https://doi.org/10.1631/FITEE.2400376) contains supplementary materials, which are available to authorized users

ORCID: Yu GAN, https://orcid.org/0009-0006-9905-6240; Hongfu MENG, https://orcid.org/0000-0003-1777-9199

OAM waves, offering the capability to generate multiple OAM modes by manipulating the excitation phase of the integrated front-end module. However, a fixed feed network within a UCA typically limits its functionality to the generation of a single OAM mode (Guo et al., 2018). In contrast, UCA antennas equipped with a reconfigurable feed network can generate multiple OAM modes. Nevertheless, these antennas are limited to generating one OAM mode at a time (Kang et al., 2019).

Existing OAM multiplexing systems, often using passive feed networks, are limited in their ability to dynamically switch between different OAM modes or reconfigure the receiving and transmitting states. These constraints restrict their practical applicability in scenarios requiring flexibility and adaptability. To address this drawback, this paper proposes a reconfigurable OAM multiplexing communication system employing active UCAs to enable simultaneous five-mode transmission.

Our system allows independent configuration of both the receiving and transmitting states for each UCA, enabling seamless switching between different OAM modes. This capability is achieved through the integration of active T/R modules, comprising beamformer ICs and feed networks. This feature is particularly advantageous in dynamic environments, where the optimal OAM mode for transmission may vary over time.

Our system is capable of simultaneous five-mode transmission, including modes 0, ±1, and ±2. This capability not only increases the overall data rate but also demonstrates the scalability of our approach. By leveraging the orthogonality of OAM modes, it can efficiently multiplex and demultiplex multiple data streams through a single pair of apertures, minimizing crosstalk and simplifying signal processing. This system is designed with dedicated antennas for each OAM mode, ensuring high isolation and purity; it is successfully tested over a 6-m link, achieving a data transmission rate of 3 Gbit/s. While the communication distance and rate may not be the highest reported to date, our focus on reconfigurability, active control, and simultaneous multi-mode transmission distinguishes this work from existing studies.

2 System design

Research on OAM multiplexing in wireless communication can be classified into five main categories: antenna design, beam generation, end-to-end experiments, signal processing methods, and system studies, such as capacity assessments and link budgets. This paper will focus on antenna design and end-to-end experiments.

2.1 Design of OAM multiplexing transceiver

To achieve a high isolation OAM multiplexing communication system, dedicated antennas are individually designed for each OAM mode. Fig. 1 presents the schematic diagram of the transceiver system

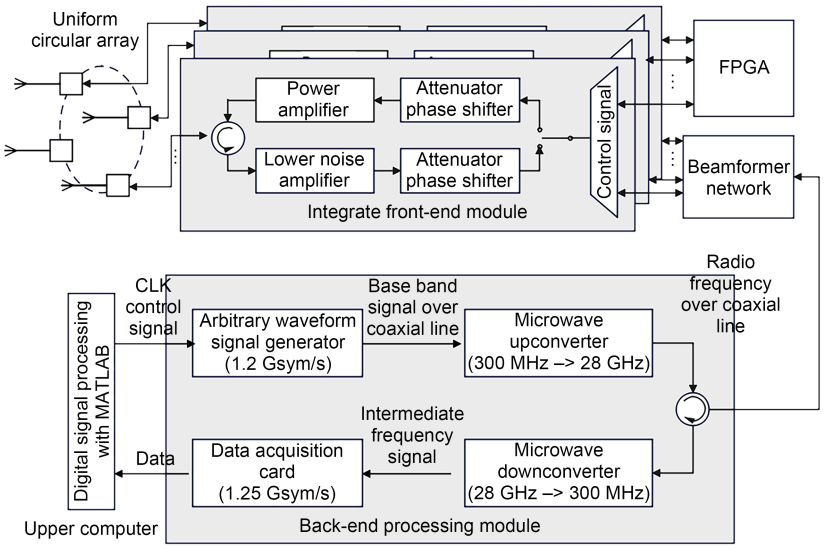

Fig. 1 Diagram of multi-mode orbital angular momentum (OAM) transceiver system

that comprises a dual-loop UCA, an integrated front-end module, a beam control board, and a back-end processing module. The front-end integration module primarily consists of beamforming chips that encompass essential functionalities such as attenuators, phase shifters, and transceiver switches. The next stage of the front-end module is the beam control board, which involves a field programmable gate array (FPGA) and a beamformer network. The beam control board emits control signals to switch OAM modes and receiving and transmitting states. This ensures that each UCA receives signals with known amplitudes, phases, and consistent timing. The reception and transmission states, as well as the radio frequency (RF) attenuator and phase shifter settings for each channel, can be rapidly switched while maintaining the selected OAM mode. The back-end processing module primarily consists of mixers and facilitates the conversion between intermediate frequency (IF) signals (300 MHz) and RF signals (28 GHz).

The transmission and reception of OAM modes +1, −1, +2, and −2 are achieved by eight subarrays as shown in Fig. 2. These eight subarrays are sufficient to produce highly pure OAM beams (Thidé et al., 2007). The number of array elements has an additional influence on an OAM-generating antenna array, compared to that of a regular antenna array, as it determines the largest mode the array can generate. In the discrete approximation used here, OAM modes with too large values of ℓ ($|\ell|\geq N/2$), where N is the number of array elements, cannot generate a pure rotating phase front and a perfect OAM mode. The beam will experience distortion and fail to maintain a stable OAM mode number across the entire conical intensity maximum profile.

2.2 System SNR and antenna metrics

The objective of this study is to facilitate the simultaneous transmission of five streams using OAM keying signals. The OAM multiplexing is implemented in the 27.5–28.5 GHz band over a distance of 6 m. Channel coding is required to achieve a signal-to-noise ratio (SNR) of more than 15 dB for error-free transmission. The receiving SNR of each mode is given in Eq. (1).

$$\mathrm{SNR}=P_{\mathrm{T}}+G_{\mathrm{T}}-P_{\mathrm{L}}+G_{\mathrm{R}}-P_{\mathrm{N}}+\mathrm{NF}, \tag{1}$$

where P_{T}, G_{T}, P_{L}, G_{R}, P_{N}, and NF represent transmitter (TX) power, TX antenna gain, path loss, receiver (RX) antenna gain, thermal noise, and noise figure, respectively. In the case of UCA-based OAM transmission, P_{L} takes the following unique values (Nguyen et al., 2018):

$$P_{\mathrm{L}}=\left|\sum_{n=0}^{N_{\mathrm{r}}-1}\sum_{m=0}^{N_{\mathrm{t}}-1}\frac{1}{\sqrt{N_{\mathrm{r}}N_{\mathrm{t}}}}\cdot\exp\left(i2\pi\ell\left(\frac{m}{N_{\mathrm{t}}}-\frac{n}{N_{\mathrm{r}}}\right)-ikr_{mn}\right)\frac{\lambda}{4\pi r_{mn}}\right|^2, \tag{2}$$

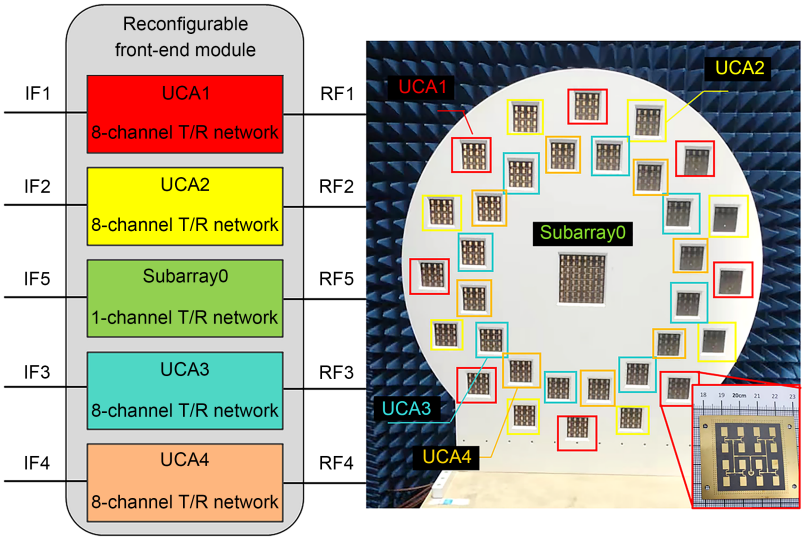

Fig. 2 Front view of OAM spatial multiplexing antenna with simultaneous five-mode transmission architecture

where N_t, N_r, k, ℓ, λ, and r_{mn} represent the number of TX antenna elements, the number of RX antenna elements, wave number, the value of OAM mode, wavelength, and the distance from element m of TX to element n of RX, respectively. Considering the experimental environment in this study, we set P_T=0 dBm, P_N=−81 dBm, and NF=6 dB. In particular, P_L is set from 63 dB to 83 dB because it varies according to the parameters of N_t, N_r, ℓ, λ, and r_{mn}. To obtain an SNR of 15 dB or higher under the highest path loss condition, which is 83 dB (Sasaki et al., 2019), the sum of TX and RX antenna gains must be equal to or higher than 22 dBi, i.e., $G_T+G_R\geq 22$ dBi. Therefore, the objective is to design antennas with a gain exceeding 11 dBi. This study proposes a narrowband 4×4 two-layer microstrip array with a gain exceeding 20 dBi. The active T/R feed network can also contribute to an additional gain. However, an excessively high gain in the T/R network may lead to system self-excitation.

Fig. 2 shows the multi-UCAs for OAM multiplexing, where four UCAs are arranged concentrically. The receiving and transmitting systems share the same structure, ensuring a symmetrical distribution of waves. The UCA consists of 4×4 microstrip antenna arrays in subarrays, which is connected to the beam-controlling printed circuit board (PCB) via a sub-miniature push-on (SMP) connector. Sixteen subarrays are uniformly distributed along the circumference in a continuous manner. Each OAM mode has eight subarrays with an additional central subarray, resulting in a total of 33 subarrays for the T/R system. The inner loop transceiver has a radius of 0.17 m, while the outer loop transceiver has a radius of 0.23 m.

2.3 Communication distance

The selection of communication distance is critical because different OAM modes exhibit distinct divergence angles. As the mode number increases, so does the divergence angle, which corresponds to the angles indicated by the two main lobes of the antenna's far-field radiation pattern. Additionally, a larger antenna aperture results in a smaller divergence angle. Consequently, the choice of communication distance must carefully consider four factors: the distribution radius of the UCA, operating frequency, OAM mode number, and divergence angle.

In the proposed system, efforts were made to ensure that the energy received by both the inner and outer antennas encompasses the majority of the OAM energy distribution. To achieve this, a method similar to near-field scanning was employed, simulating the field distribution of various OAM modes within cross-sections at different distances. The objective was to design transmitting and receiving antennas with identical apertures and symmetrical configurations, facilitating seamless switching between modal transmission and reception while capitalizing on the benefits of the active T/R feed network. Ideally, the OAM field distribution emitted from the inner antenna should attain its maximum amplitude precisely at the inner position of the receiver antenna. Similarly, the transmitting and receiving antennas of the outer ring should produce the strongest field amplitude at the same location, ensuring optimal energy transfer efficiency throughout the communication system.

In this example, the frequency, UCA size, and distance between TX and RX antennas were set to 28 GHz, 0.5 m, and 10 m, respectively. Since the diffraction pattern of the UCA can be approximated as a Bessel beam (Tian et al., 2016), the OAM intensity generated by the UCAs has different peaks at different distances, the distribution of which is given by Eq. (3).

$$v_L(r,\theta,z)=\frac{\lambda\exp\left[\left(\frac{2\pi i}{\lambda}\right)\sqrt{r^2+z^2}\right]}{4\pi\sqrt{r^2+z^2}}\cdot i^{-\ell}e^{i\ell\theta}\cdot J_\ell\left(\frac{2\pi rD}{\lambda\sqrt{r^2+z^2}}\right), \tag{3}$$

where J_ℓ, λ, and D denote the ℓ^{th}-order Bessel function of the first kind, the wavelength of the carrier frequency, and the radius of the transmitting UCA, respectively. (r,θ,z) refers to cylindrical coordinates, where r and θ are the radius and azimuthal angle at the RX plane, respectively, and z is the distance between the TX and RX UCAs. In this design, the electric field is polarized in the y-direction and propagates along the z-axis. Fig. 3 illustrates the magnitudes of the Bessel distribution electric field with different modes in the line y=0 on the cross-section plane, 10 m from the antenna.

From the TX perspective, this allows different OAM modes to be transmitted using different UCAs to avoid the null region at the RX antenna. Each subarray contributes one OAM mode, which is fed by an

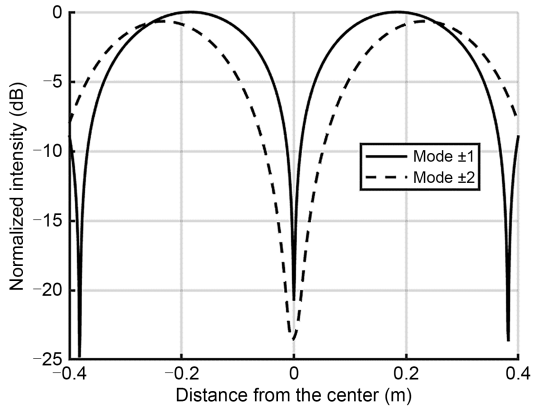

Fig. 3 Simulation of intensity distributions of transmitter (TX) signals. Frequency: 28 GHz; radius of TX loop-1 and loop-2 UCA: 0.17 m/0.23 m; distance between TX and receiver (RX): 10 m

independent channel. This also enables the transmission of multiple sets of the same OAM mode. From the RX perspective, multiple UCAs provide increased freedom, enabling the RX antenna to receive most of the energy. Our transmitting and receiving antennas share an identical structure, which not only reduces manufacturing costs but also ensures symmetry.

Based on the aforementioned conclusions, the system sets the communication distance within a range of 6 m to 10 m. Despite sacrificing communication distance, it attains the benefits of seamless switching between transmit and receive modes and high energy utilization efficiency, making it more suitable for practical duplex system applications. Given that the presented system primarily serves as a verification system for OAM communication, considering the impact of OAM multipath effects and OAM purity, we have determined an experimental distance of 6 m. In future work, we will focus on enhancing design and experimental methodologies for long-distance communication.

In contrast to other studies, the communication system distance reported in this paper does not exhibit notable superiority. As such, future research should prioritize enhancing communication distance. Approaches to increase the communication distance include enlarging the antenna aperture, augmenting the number of channels, enhancing the RF link gain, special beam shaping, lowering the noise coefficient, and implementing algorithmic compensation for restoring the OAM field.

2.4 Phase calibration of UCA

As shown in Fig. 4a, an open waveguide probe is scanned along a circular trajectory using a vector network analyzer (VNA) and a scanning frame. At a distance of three wavelengths from the surface of the antenna array, phase measurements are conducted for each element, after which the digital phase shifter is calibrated to excite signals with uniformly distributed phase differences corresponding to the OAM mode number. The results before and after phase calibration are shown in Table 1. The phase intervals after

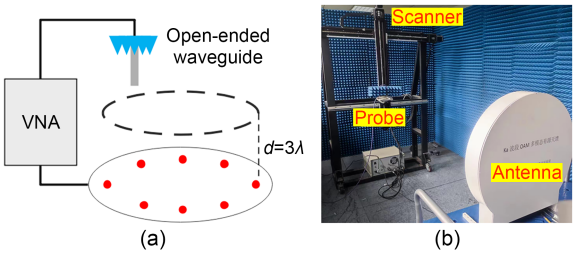

Fig. 4 Diagram of near-field phase calibration (a) and photo of near-field measurement scenarios (b)

Table 1 Comparison of phase calibration results for eight channels

	ℓ	Forward transmission coefficient (degree)							
		CH1	CH2	CH3	CH4	CH5	CH6	CH7	CH8
Before calibrating	+1	113	−123	169	165	−5	108	−129	−28
	−1	56	−167	126	156	64	93	88	−39
	+2	−22	−43	96	106	−113	−4	−20	53
	−2	75	92	−81	65	56	−121	−137	−1
After calibrating	+1	1	47	87	139	−173	−129	−85	−48
	−1	6	−44	−85	−134	179	135	96	51
	+2	−88	0	91	176	−94	2	89	176
	−2	143	47	−44	−129	143	51	−36	−142

Taken from data captured by vector network analyzer (VNA) at 28 GHz

calibration are not strictly equal due to the limited precision of the digital phase shifter and the possibility that the scanning plane may not be perfectly parallel to the array surface.

The state after phase calibration is recorded as a standard excitation file, and different OAM modes are switched as needed. In the next section, OAM modes are mapped to different UCAs based on this, and near-field measurements are performed at a greater distance using a scanner, as shown in Fig. 4b. The calibrated results exhibit a non-uniform phase interval distribution; however, the simulated phase distribution of the calibrated OAM mode incorporates the phase error within the prescribed tolerance range. Subsequently, this distribution is compared with the ideal phase distribution, revealing that inter-modal interference caused by a ±10° phase error is attenuated to less than 30 dB.

To alleviate the influence of multipath effects, the experimental scenario of this paper elevates the antenna as far from the ground as possible, ensuring that the lower edge of the antenna is 1.5 m above the ground. Based on a simple assessment, the cross-interference of multipath effects on the main OAM mode can be minimized to less than 15 dB in coordination with the absorbing material plates on both sides. As the number of OAM modes is relatively small and the impact of non-line-of-sight (NLoS) is relatively minor, its influence is temporarily disregarded in this experiment.

3 OAM spectrum measurement

The near-field data allow us to assess the errors in amplitude and phase distribution of the generated OAM beams, which is crucial for understanding the fidelity of the OAM modes and ensuring the accuracy of our communication system. By comparing the measured data with theoretical predictions, we can identify any deviations that may result from imperfections in the antenna design or transmission medium. The purity of the OAM modes is a critical metric for the performance of OAM-based communication systems. By analyzing the near-field distributions, we can evaluate the purity of the generated OAM beams. For instance, in our study, we observed that the amplitude distribution of the second-order OAM beam is not perfectly uniform, indicating potential imperfections in the generation process.

To observe the purity of the emitted electromagnetic vortex waves and the OAM spectrum, it is necessary to establish an experimental environment capable of testing the near field. As shown in Fig. 4b, a two-dimensional motion controller is used to move the open-ended waveguide probe within a plane parallel to the antenna's aperture. After achieving the desired positioning, amplitude and phase data of the electric field are recorded using a VNA.

In the near-field measurement and communication experiments, the outer UCAs (UCA1 and UCA2) are configured to receive and transmit OAM modes ±2, while the inner UCAs (UCA3 and UCA4) are configured to receive and transmit OAM modes ±1. The central array receives and transmits plane waves.

The measured transverse electric field magnitude and phase distributions for the first-order and second-order OAM beams are shown in Fig. 5. Figs. 5a, 5c, 5e, and 5g show the magnitude distributions in the *xoy*-plane at a distance of 6 m, while Figs. 5b, 5d, 5f, and 5h show the phase distributions.

The near-field measurement results provide valuable insights into the performance of our OAM multiplexing communication system. Quantitatively, it is observed that the field strength maximum energy radii for the modes ±1 and ±2 at a distance of 6 m are approximately 100 mm and 138 mm, respectively. The amplitude distribution on the loop of the second-order OAM beam is not uniform. This discrepancy may arise from variations in output power among different channels of the T/R chip or potential distortions caused by bending in the coaxial line. To mitigate systematic errors and compensate for loss disparities, the T/R boards undergo calibration using a VNA. Due to the limitations in attenuator accuracy (±1 dB) and phase shifter accuracy (±11.25°), complete consistency across all channels is unattainable. These values align well with the modal distribution discussed in Section 2.3 for a distance of 10 m, indicating that the majority of the energy is confined within the aperture distribution of the receiving antenna. This confirms that our system design enables efficient energy transmission over the selected communication distance. The phase distributions in the near field exhibit a fork-like pattern, indicating potential misalignment between the measurement plane and the emitting

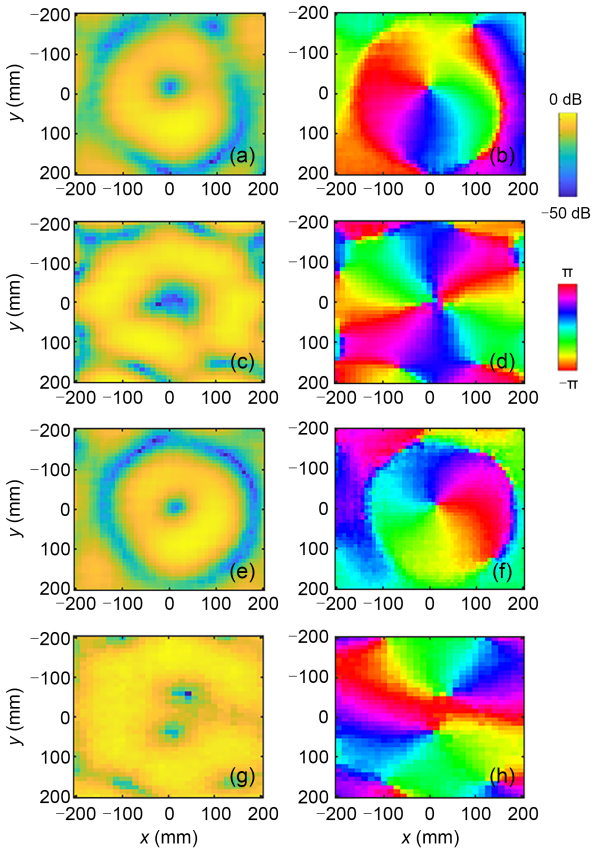

Fig. 5 Measured transverse electric field intensity of generated OAM modes +1 (a), +2 (c), −1 (e), and −2 (g); measured phase distributions with OAM modes +1 (b), +2 (d), −1 (f), and −2 (h)

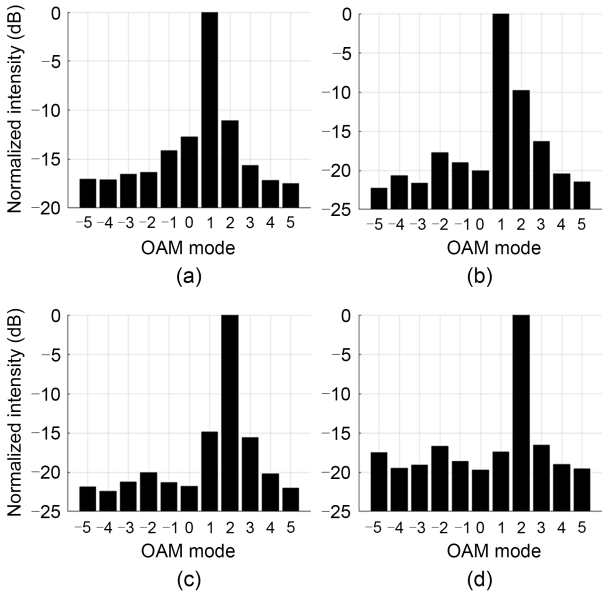

Fig. 6 Measured OAM spectrum of proposed system with four non-zero OAM streams: (a) TX mode +1; (b) RX mode +1; (c) TX mode +2; (d) RX mode +2

antenna aperture. Attitude sensitivity poses a common challenge in OAM testing, and the presented phase data represent raw measurement results. Although compensating for angular errors post-measurement could enhance accuracy, it requires a standard OAM generator and planar calibration system, which are unavailable under our experimental conditions. Instead, this work employed mechanical parallel calibration methods to ensure that any misalignment between the measurement plane and the antenna aperture does not exceed 2°, thereby minimizing its impact on our measurements.

The OAM spectrum can be calculated by measuring the amplitude and phase of the electric field using the near-field test results shown in Fig. 5. The measured OAM spectrum is presented in Fig. 6, calculated by Eqs. (4) and (5).

$$a_\ell(r,z)=\frac{1}{\sqrt{2\pi}}\sum_{\ell=-\infty}^{+\infty}a_\ell(r,z)\cdot\exp(i\ell\varphi), \tag{4}$$

where the helical harmonic $\exp(i\ell\varphi)$ is the eigen wave function of OAM with the complex coefficient a_ℓ. Thus, the intensity of the ℓ^{th}-order helical harmonic is:

$$C_\ell(r,z)=\int_0^{+\infty}\left|a_\ell(r,z)\right|^2 r\mathrm{d}r. \tag{5}$$

Additionally, the influence of NLoS paths becomes more significant at greater distances. However, reducing the communication distance solely to improve purity is not feasible due to the OAM spatial filtering effect, which causes a significant portion of the energy to be reflected within the inner region instead of being fully received by the antenna. This is pivotal for grasping the likelihood of cross-talk between OAM channels and refining system design to alleviate such interference. The envelope of the OAM spectrum follows the Singer function, resulting in lower isolation between contiguous OAM modes compared to other modes. In this study, the measured isolation of all modes is below 10 dB. Moving forward, optimization efforts will be focused on modes with inadequate isolation, with a primary emphasis on enhancing the design of feed networks and refining calibration methodologies to achieve an isolation level exceeding 10 dB for all modes.

4 Communication experiment

The same OAM configuration from the previous near-field measurement was applied, with the outer UCA configured to receive and transmit OAM modes ±2, the inner UCA for OAM modes ±1, and the central array receiving and transmitting plane waves. For the same OAM transmission mode, different modes were used to receive and measure the power in the intermediate frequency, using a spectrum analyzer. The results were normalized and organized into Table 2. The matched OAM mode showed higher power in the intermediate frequency than the mismatched mode, as shown in Fig. 7.

Table 2 Normalized power measured by signal analyzer on intermediate frequency (IF) band

RX mode	IF power (dB)				
	TX mode=+1	−1	+2	−2	0
−1	0	−9.4	−10.4	−14.8	−8.4
+1	−10.9	0	−10.8	−11.8	−18.2
−2	−11	−16.2	0	−10.7	−5.6
+2	−5	−17.6	−6.8	0	−5
0	−25.3	−11.8	−20.6	−11.6	0

Data taken from Agilent spectrum analyzer E4447A

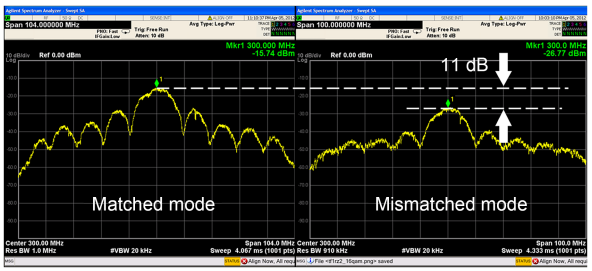

Fig. 7 TX OAM mode-checking: an 11-dB difference in intermediate frequency (IF) power. The TX mode is +1 while the RX UCA is −1 (matched) and +1 (mismatched)

This experimental platform uses a data acquisition card and an arbitrary waveform generator. The communication setup is shown in Fig. 8. The arbitrary waveform generator directly generates an intermediate frequency signal (300 MHz), radiated at 28 GHz through the upconverter and T/R board. Similarly, the receiving antenna performs post-processing on the received signal through down-conversion and T/R. The waveform of the data at the transmitting end is shown in Fig. 9a, while the waveform received at the receiving end is shown in Fig. 9b. The sampling rates of the arbitrary waveform generator and the data acquisition card are 1.2 GS/s and 1.25 GS/s, respectively. At the input of the frequency conversion daisy chain, up- or down-converters that are cascaded through a coaxial line are used to convert the input signal of 300 MHz to 28 GHz. In the proposed system, the data acquisition card collects 512 kS of data, which are then sent to the upper computer. MATLAB is used on the computer to demodulate the collected data, recover user data, and display the constellation diagram. The error vector magnitude performance is measured with quadrature phase shift keying (QPSK), 16-QAM, and 64-QAM waveforms in RX mode. The experimental results of the OAM communication data streams of the five modes at the receiving end are shown in Fig. 10. The error vector magnitude contributors include external components such as PCB-based transmission lines, cross-polarization of the antenna, OAM mode purity, antenna orientation angles, and bonding wires.

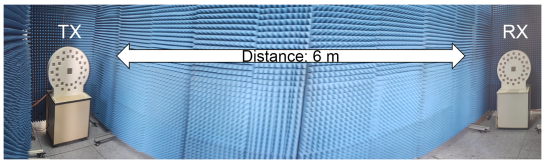

Fig. 8 Communication measurement setup

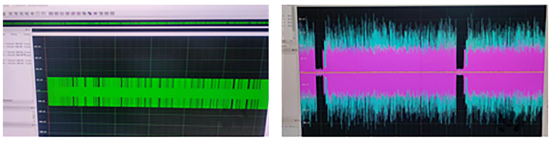

Fig. 9 Transmitting (a) and receiving (b) waveform

After completing the constellation display, the data acquisition card is controlled for data collection. This process cannot fully collect the transmitted data, and the collection interval can be approximated as the demodulation time of the upper computer. Due to the randomness of the data collection starting point, the data are accurately demodulated, and it is necessary to determine the starting position of each frame of data. At the same time, to balance the collection rate, an all-zero sequence is added before the pilot sequence to estimate the data frame's starting position. In this

experiment, the data frame consists of an all-zero sequence, a pilot sequence, and a user data sequence, with a ratio of 49:14:512.

The OAM multiplexing communication experiment is summarized in Table 3. The active T/R employs a phase shifter and attenuator chip instead of the Butler matrix as the feed network. Compared to the communication system mentioned in the reference paper, the system designed in this paper has the advantages of simultaneous multi-mode transmission and reception, transmission-reception state reciprocity, and flexible and reconfigurable OAM mode.

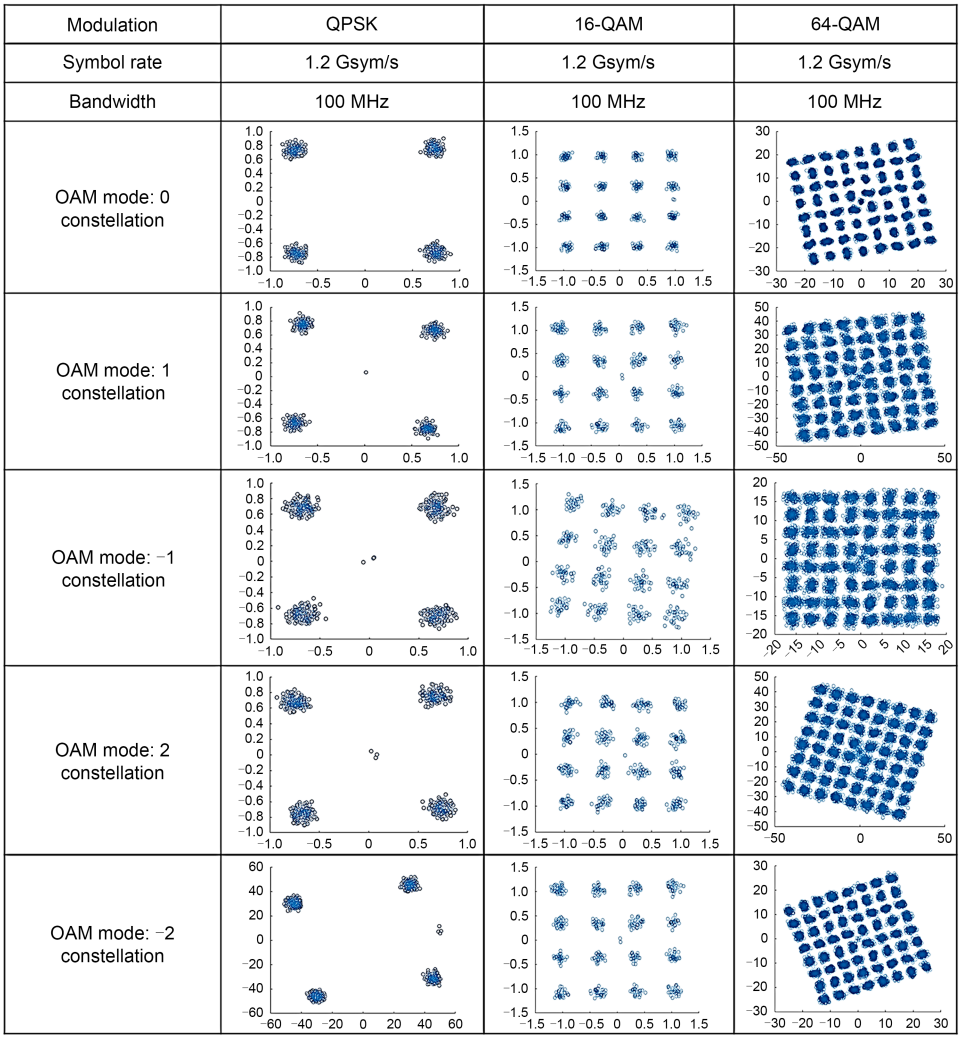

Fig. 10 Constellation diagrams with five streams (0, ±1, ±2) simultaneous communication

Table 3 Comparison with other OAM multiplexing communication systems

Reference	Method	Frequency	Propagate distance	OAM mode	Speed	Type of feed network
Yan et al. (2014)	SPP	28 GHz	2.5 m	±1, ±3	32 Gbit/s	Passive
Tamburini et al. (2015)	Parabolic reflector	17 GHz	150 m	0, ±1	33 Mbit/s	Passive
Yan et al. (2016)	SPP	60 GHz	15 cm	±1, ±2	8 Gbit/s	Passive
Nguyen et al. (2018)	UCA	74.5 GHz	7 m	0, ±1, ±2, ±3, ±4	3.2 Gbit/s	Passive
Lee et al. (2018)	UCA	28 GHz	10 m	0, ±1, ±2	200 Gbit/s	Passive
This paper	UCA	28 GHz	6 m	0, ±1, ±2	3 Gbit/s	Active

SPP: spiral phase plate; UCA: uniform circular array

5 Conclusions

A 6-m OAM link is designed to enable the simultaneous transmission of five OAM streams, achieving a transmission rate of 3 Gbit/s. There is still significant room for improvement in this communication system. In this experiment, the communication rate is primarily limited by the relatively small intermediate frequency bandwidth. Both the frequency conversion module and T/R module have a large gain margin. Future work may involve designing longer communication links, addressing the OAM divergence angle, and exploring its potential for high-speed and long-distance communication.

Contributors

Yu GAN designed the research. Yu GAN and Lin LIU processed the data and performed the experiments. Yu GAN drafted the paper. Hongfu MENG and Jian BAI helped organize the paper. Yu GAN and Hongfu MENG revised and finalized the paper.

Conflict of interest

All the authors declare that they have no conflict of interest.

Data availability

The data that support the findings of this study are available from the corresponding author upon reasonable request.

References

Cheng Q, Jin S, Cui TJ, 2023. Reconfigurable intelligent surfaces for wireless communications. *Front Inform Technol Electron Eng*, 24(12):1665-1668. https://doi.org/10.1631/FITEE.2320000

Gesbert D, Shafi M, Shiu DS, et al., 2003. From theory to practice: an overview of MIMO space-time coded wireless systems. *IEEE J Sel Areas Commun*, 21(3):281-302. https://doi.org/10.1109/JSAC.2003.809458

Gibson G, Courtial J, Padgett MJ, et al., 2004. Free-space information transfer using light beams carrying orbital angular momentum. *Opt Express*, 12(22):5448-5456. https://doi.org/10.1364/OPEX.12.005448

Guo ZG, Yang GM, Jin YQ, 2018. Circularly polarised OAM antenna using an aperture-coupled uniform circular array. *IET Microw Antenn Propag*, 12(9):1594-1600. https://doi.org/10.1049/iet-map.2017.1126

Kang L, Li H, Zhou JZ, et al., 2019. A mode-reconfigurable orbital angular momentum antenna with simplified feeding scheme. *IEEE Trans Antenn Propag*, 67(7):4866-4871. https://doi.org/10.1109/TAP.2019.2916595

Lee D, Sasaki H, Fukumoto H, et al., 2018. An experimental demonstration of 28 GHz band wireless OAM-MIMO (orbital angular momentum multi-input and multi-output) multiplexing. Proc 87th Vehicular Technology Conf, p.1-5. https://doi.org/10.1109/VTCSpring.2018.8417790

Nguyen T, Hirabe M, Miyamoto H, et al., 2018. An experimental study of high-capacity link using orbital angular momentum mode multiplexing in E-band. Proc Int Symp on Antennas and Propagation, p.1-2.

Qiu LJ, Li XP, Qi ZH, et al., 2023. Wideband circular-polarized transmitarray for generating a high-purity vortex beam. *Front Inform Technol Electron Eng*, 24(6):927-934. https://doi.org/10.1631/FITEE.2200539

Sasaki H, Yagi Y, Yamada T, et al., 2019. Field experimental demonstration on OAM-MIMO wireless transmission on 28 GHz band. Proc IEEE Globecom Workshops, p.1-4. https://doi.org/10.1109/GCWkshps45667.2019.9024684

Tamburini F, Mari E, Parisi G, et al., 2015. Tripling the capacity of a point-to-point radio link by using electromagnetic vortices. *Radio Sci*, 50(6):501-508. https://doi.org/10.1002/2015RS005662

Thidé B, Then H, Sjöholm J, et al., 2007. Utilization of photon orbital angular momentum in the low-frequency radio domain. *Phys Rev Lett*, 99(8):087701. https://doi.org/10.1103/PhysRevLett.99.087701

Tian H, Liu ZQ, Xi W, et al., 2016. Beam axis detection and alignment for uniform circular array-based orbital angular momentum wireless communication. *IET Commun*, 10(1): 44-49. https://doi.org/10.1049/iet-com.2015.0136

Yan Y, Xie GD, Lavery MPJ, et al., 2014. High-capacity millimetre-wave communications with orbital angular momentum multiplexing. *Nat Commun*, 5(1):4876. https://doi.org/10.1038/ncomms5876

Yan Y, Li L, Zhao Z, et al., 2016. 32-Gbit/s 60-GHz millimeter-wave wireless communication using orbital angular momentum and polarization multiplexing. Proc IEEE Int Conf on Communications, p.1-6. https://doi.org/10.1109/ICC.2016.7511277

Yang LJ, Sun S, Sha WEI, et al., 2023. Multi-feed multi-mode metasurface for independent orbital angular momentum communication in dual polarization. *Front Inform Technol Electron Eng*, 24(12):1776-1790. https://doi.org/10.1631/FITEE.2200471

Yousif BB, Elsayed EE, Alzalabani MM, 2019. Atmospheric turbulence mitigation using spatial mode multiplexing and modified pulse position modulation in hybrid RF/FSO orbital-angular-momentum multiplexed based on MIMO wireless communications system. *Opt Commun*, 436:197-208. https://doi.org/10.1016/j.optcom.2018.12.034

Zhang Q, Xiong XS, Li Q, et al., 2021. Modeling and performance analysis of OAM-GSM millimeter-wave wireless communication systems. *Front Inform Technol Electron Eng*, 22(4):527-547. https://doi.org/10.1631/FITEE.2000444

List of supplementary materials

1 Supplement to the analysis of non-line-of-sight (NLoS) conditions

2 Supplement to the analysis of non-uniform phase calibration

3 Supplement to the measurement of near field with different distance

Fig. S1 Multipath effects of an OAM channel caused by specular reflection from a parallel ideal reflector

Fig. S2 Simulation results showing the intensity, phase, and OAM spectrum of the direct path OAM beam, reflected path OAM beam, and the actual beam at the receiver

Fig. S3 Analysis of OAM interference between ideal phase distribution and actual phase distribution

Fig. S4 Measured electric field intensity and measured phase distribution of different OAM modes

Table S1 Comparison of calibrated phase distribution with ideal phase distribution